

RESEARCH ARTICLE

10.1029/2018TC005079

Key Points:

- The topographical contributions from crust, mantle lithosphere, mantle composition, and asthenospheric flow are estimated
- East of the TGB the lithosphere is thin, suggesting much of eastern China has experienced lithospheric dismemberment
- Widespread positive dynamic topography seems unlikely in east China

Correspondence to:

Y. Deng,
yangfandeng@gig.ac.cn

Citation:

Deng, Y., & Levandowski, W. (2018). Lithospheric alteration, intraplate crustal deformation, and topography in eastern China. *Tectonics*, 37. <https://doi.org/10.1029/2018TC005079>

Received 29 MAR 2018

Accepted 11 OCT 2018

Accepted article online 16 OCT 2018

Lithospheric Alteration, Intraplate Crustal Deformation, and Topography in Eastern China

Yangfan Deng¹  and Will Levandowski² 

¹State Key Laboratory of Isotope Geochemistry, Guangzhou Institute of Geochemistry, Chinese Academy of Sciences, Guangzhou, China, ²TetraTech, Inc., Golden, CO, USA

Abstract Topography can be directly observed, but what controls topographic variation is not readily known. To investigate a prominent and remarkably consistent along-trend topographic gradient belt (TGB) in intraplate eastern China and its connection to ongoing deformation and geodynamics, we examine the regional density structure of the crust and mantle lithosphere. We first use S velocities to derive an initial density and then refine the density model by joint inversion of topography and gravity. We use the final density model and receiver functions to strip away topographic contributions from the crust, and we subsequently estimate the thickness of the mantle lithosphere required to satisfy flexural isostasy. Crustal buoyancy overcompensates for the elevation change across the TGB. East of the TGB (eastern north China craton and southeastern south China), the lithosphere is thin (~90 km), suggesting that not only the eastern north China craton but also much of the eastern China has experienced lithospheric dismemberment. The TGB behaves as an important contour for the lithospheric thickness, except for the northeast China and Qinling-Dabie. Proposed refertilization of the altered mantle lithosphere in the east side of TGB would result in even lower lithospheric thickness, while hydration and asthenosphere upwelling have the opposite effect. This systematic calculation gives a regional analysis of eastern China and could be a useful guide for the regions lacking seismic investigations.

1. Introduction

Topography is a ubiquitous geophysical observable, and because relief arises—albeit nonuniquely—from the temperature, composition, and flexural strength of the lithosphere and flow in the asthenosphere, determining the physical origin of topography can provide insight both into thermochemical structure and into dynamics. It can be challenging, however, to understand tectonic history and ongoing dynamics in continental interiors where the processes normally associated with orogeny are not active or have long since ceased. In addition to boundaries of the Tibetan plateau, mainland China hosts another remarkable topographic gradient belt (TGB) that, consistently for ~4,000 km along-strike, separates ~100-m elevations to the east from >1-km elevations to the west (Figure 1). The TGB coincides with a similarly pronounced gravity gradient belt, the North-South Gravity Lineament (NSGL), which has been proposed to reflect an intracontinental boundary between not only topographically but also tectonically different domains (Menzie & Xu, 1998; Kusky et al., 2007; Xu, 2007; Zheng et al., 2007).

These observations across the TGB are well studied in the north China craton (NCC). The entire NCC had a thick root in the Precambrian and Paleozoic but experienced large-scale root loss in the Mesozoic, with hypothesized mechanisms for this loss ranging from large-scale delamination or density-driven foundering to thermal erosion such as by melt-peridotite reactions (e.g., Foley, 2008; Gao et al., 2009; Zhang, 2005). Seismological observations and mantle xenoliths suggest that the boundary between the thinned lithosphere of the east north China craton (ENCC) (Chen et al., 2009; Zhang et al., 2014; Zhu et al., 2012) and the stable Ordos basin and west north China craton (WNCC) coincides approximately with the TGB. Indeed, the mantle to the west of the TGB is older (late Archean-early Proterozoic) than that beneath the eastern NCC, where the thick, old, and refractory lithospheric keel was replaced by a thin, young, and fertile mantle in a process related to the widespread lithospheric extension in the eastern NCC after the late Mesozoic (Xu, 2007; Zheng et al., 2007).

The contrast in lithospheric properties between the ENCC and WNCC is well studied, and the fact that the boundary between the two is roughly coincident with the TGB has been established (Chen et al., 2008, 2009); it is not known, however, whether the physiographic boundary defined by the TGB is a tectonothermal

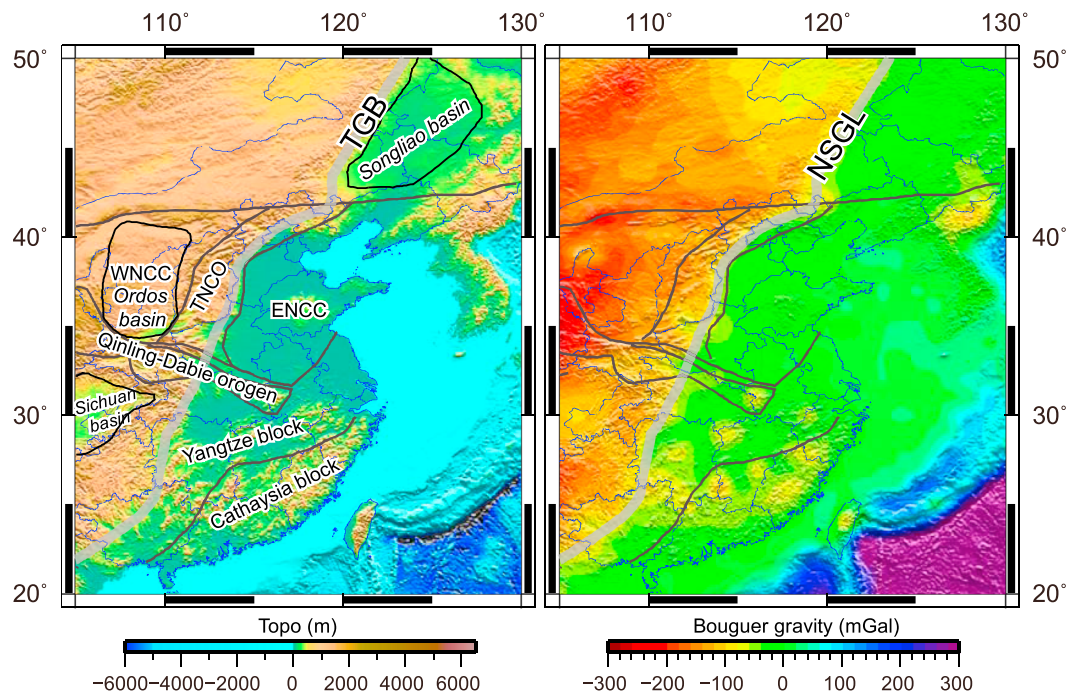


Figure 1. (left) Topography (Etopo1, Amante & Eakins, 2009) and (right) Bouguer gravity (EGM2008, Pavlis et al., 2012) of east China. TGB = topographic gradient belt; NSGL = north-south gravity lineament; ENCC = east north China craton; TNCO = trans-north China orogen; WNCC = west north China craton.

boundary elsewhere along strike. On one hand, surface heat flow is indeed generally higher to the east than the west (Jiang et al., 2016, Figure 2d). On the other, intraplate volcanism occurs on either side, especially in northern China (e.g., Datong volcano, Honggeertu volcano, Changbaishan volcano, Jingbo volcano, Longgang volcano, Arshan volcano, Wudalianchi volcano, Keluo volcano; Figure 2b), which calls into question a consistent difference in the thermochemical structure of the lithosphere east and west of the TGB.

To explore the origin of the TGB—and more broadly the structure of the lithosphere in eastern China and its connection to intraplate volcanism and seismicity—we attempt to disentangle the relative contributions to surface elevation from the crust, the temperature and chemistry of the mantle lithosphere (ML), and flow in the asthenosphere. To do so, we leverage previous studies of *P* and *S* wave velocity, crustal temperature, and crustal thickness. Specifically, we estimate the initial density from *S* wave velocity (Shen et al., 2016) and refine the density model to quantify its contribution to gravity anomaly and surface elevation, accounting for the flexural strength of the lithosphere. Remaining topography is ascribed to the mantle (temperature/thickness and also possibly compositional variations and the impact of mantle flow). Next, we estimate the temperature at the Moho, the depth of which is constrained by receiver functions (Y. Li et al., 2014), from a crustal temperature model derived from borehole heat flow, *P* velocity, and 3-D thermal modeling (Sun et al., 2013). Then, we determine the thickness of the ML under the assumptions of flexural isostasy and a linear geotherm from the Moho to the lithosphere-asthenosphere boundary. Finally, we discuss the impacts of flow in the asthenosphere (which we term dynamic topography), hydration, and lithospheric compositional variations.

2. Methods and Data

2.1. Method

We largely follow the method applied by Gvirtzman et al. (2016) in the Europe/Asia/Arabia/Africa region, which begins by compiling a crustal thickness map and removing the contribution of the crust from the observed elevation. Remaining topography is ascribed to the ML. Unlike the uniform crustal density used by Gvirtzman et al. (2016), however, we use a 3-D density model (from the surface to 150-km depth) derived from joint inversion of topography and gravity. We also consider lithospheric flexure instead of local isostasy.

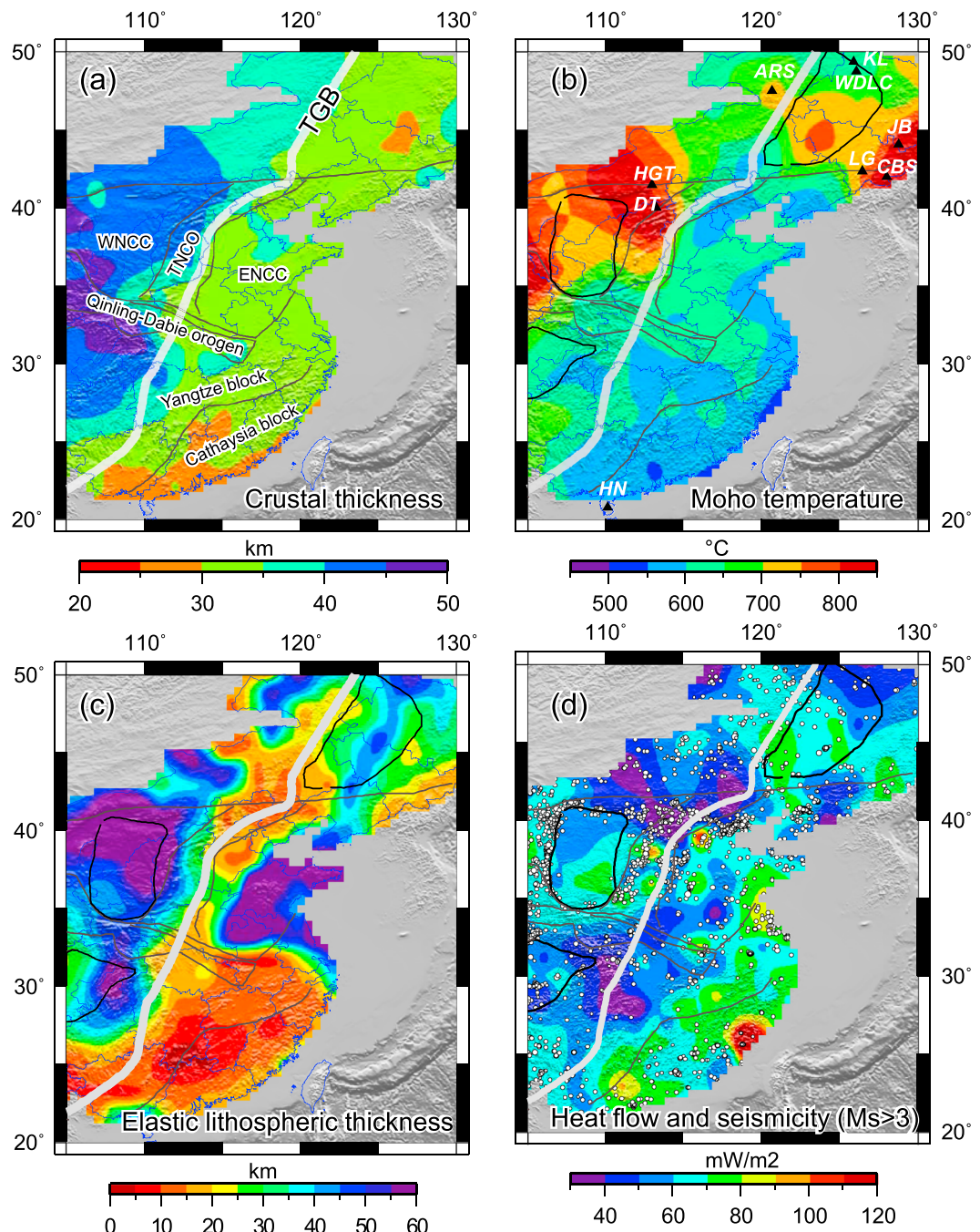


Figure 2. (a) Moho depth (Y. Li et al., 2014). (b) Moho temperature (Sun et al., 2013). The black triangle indicates the volcanos. DT = Datong volcano; HGT = Honggeertu volcano; CBS = Changbaishan volcano; JB = Jingbo volcano; LG = Longgang volcano; ARS = Arshan volcano; WDLC = Wudalianchi volcano; KL = Keluo volcano; TGB = topographic gradient belt; ENCC = east north China craton; TNCO = trans-north China orogen; WNCC = west north China craton. (c) Elastic thickness used in the topographic estimation. (d) Surface heat flow (Jiang et al., 2016) and seismicity ($M_s > 3$) since 1980 (earthquake catalog edited by the China Earthquake Network Center).

2.1.1. Isostatic Topography

The observed topography E consists of isostatic topography and dynamic topography.

$$E = H_{\text{isostatic}} + H_{\text{dynamic}} \quad (1)$$

E is interpolated from ETOPO1, a 1 arc-minute global model that integrates land topography and ocean bathymetry (Amante & Eakins, 2009).

In cases of local isostasy (without H_{dynamic} or lithospheric flexural strength) $H_{\text{isostatic}}$ is the sum of contributions from the crust (H_c) and the ML (H_{ml}). Equation (1) can be expanded as (following Lachenbruch & Morgan, 1990)

$$H_{\text{isostatic}} = H_c + H_{\text{ml}} - H_0 \quad (2)$$

H_0 is a correction term of 2.4 km to achieve isostatic equilibrium with an asthenospheric column (via mid-ocean ridges).

H_c and H_{ml} , the isostatic contribution from the ML, are the depth integrals of density contrasts between the crust and the ML, respectively, and the compensating asthenosphere:

$$H_c = \int_{\text{topo}}^{\text{Moho}} \frac{1}{\rho_a} (\rho_a - \rho_c) dz \quad (3)$$

$$H_{\text{ml}} = \frac{1}{\rho_a} (\rho_a - \rho_{\text{ml}}) T_{\text{ml}} \quad (4)$$

Here $\rho_a = 3,200 \text{ kg/m}^3$ is the density of asthenosphere; ρ_c is the crustal density; ρ_{ml} and T_{ml} are the mean density and the thickness of the ML, which we derive as follows.

In the case of local isostasy, we can rearrange equations (2) and (4) to yield

$$H_{\text{ml}} \approx E - (H_c - H_0) \quad (5)$$

$$T_{\text{ml}} = \frac{\rho_a}{(\rho_a - \rho_{\text{ml}})} [E - (H_c - H_0)] \quad (6)$$

We will discuss the roles of dynamic topography and the composition of the ML in section 4, but the thermal component of H_{ml} depends on the temperature of the ML relative to (warmer) asthenosphere (Gvirtzman et al., 2016; Parsons & Sclater, 1977). In equation (4), ρ_{ml} of material at average temperature θ_{ml} is

$$\rho_{\text{ml}} = \rho_a [1 + \delta(\theta_a - \theta_{\text{ml}})], \quad (7)$$

where θ_a is the temperature of the asthenosphere and δ is the volumetric coefficient of thermal expansion. In this study, we use $\theta_a = 1350^\circ\text{C}$ and $\delta = 4.0 \times 10^{-5}/^\circ\text{C}$ (Katsura et al., 2009). Assuming a linear geotherm for the ML from the Moho at temperature θ_c to the lithosphere-asthenosphere boundary at temperature θ_a (Gvirtzman et al., 2016), the average temperature of the ML is simply

$$\theta_{\text{ml}} = \frac{1}{2} (\theta_c + \theta_a) \quad (8)$$

Substituting equation (8) into equation (7) and then that result into equation (6) gives a single equation that estimates the thickness of the ML from the surface elevation, the crustal component of topography, and the temperature at the Moho:

$$T_{\text{ml}} = -\frac{2}{\delta(\theta_a - \theta_c)} [E - (H_c - H_0)] = \frac{2}{\delta(\theta_a - \theta_c)} [-E + (H_c - H_0)] \quad (9)$$

2.1.2. Lithospheric Flexure

The strength of the lithosphere modulates the surface topography produced by subsurface density variations (Watts, 2001), and it also supports short-wavelength topography that may exceed or fall short of the local isostatic elevation. That is, the flexural filter F must be convolved with each side of equation (1), and it follows that

$$E * F = [H_c + H_{\text{ml}} - H_0] * F \quad (10)$$

$$T_{\text{ml}} \approx \frac{2}{\delta(\theta_a - \theta_c)} [H_c - E - H_0] * F \quad (11)$$

F can be represented by a system of zero-order Kelvin-Bessel functions (Watts, 2001; his equations 3.54 and 3.55) dependent on the elastic thickness (via flexural rigidity). For the present work, we derive a new 2-D

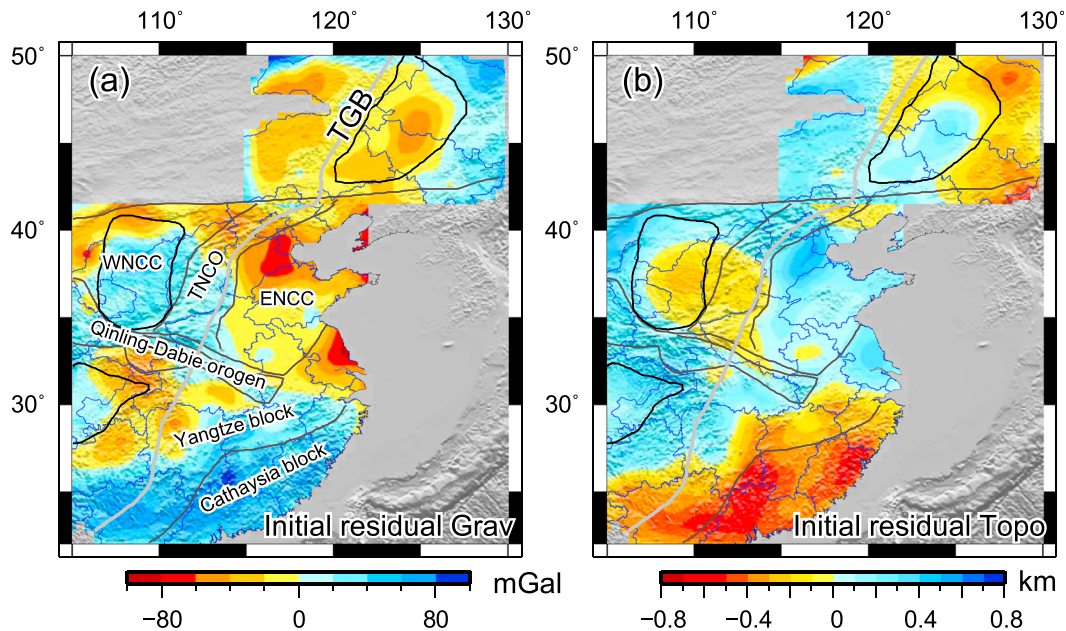


Figure 3. Residual topography and gravity attendant to the initial, seismically derived model. Negative residual topography (warm colors) denotes regions in which the densities estimated from seismic velocity are too high; negative residual gravity denotes regions in which the initial densities are too low. TGB = topographic gradient belt; ENCC = east north China craton; TNCO = trans-north China orogen; WNCC = west north China craton.

elastic thickness model of the study area by the multitaper spectral estimation method (Pérez-Gussinyé et al., 2004). We defer discussion of the features of this model to section 2.2.4.

2.2. Data

2.2.1. Crustal Density Model

Rather than a constant value for crustal density (ρ_c in equation (3)), we use a fully 3-D model derived from joint inversion for topography and gravity (Deng et al., 2017; Levandowski et al., 2015). First, we use the 3-D shear wave velocity (Shen et al., 2016) and the empirical relations of Brocher (2005) for the crust and Levandowski et al. (2015) for the mantle to construct the initial 3-D density model to 150 km (equations (12) and (13)). And then, we refine the density model by joint inversion for the topography and gravity anomalies (see more details in Levandowski et al., 2015). It should be noted that even though a stagnant slab may be widely distributed in east China (Huang & Zhao, 2006), the slab is of near-neutral buoyancy due to the low density phases offset by low temperature (King et al., 2015). Therefore, its impacts (as that of other variations near the mantle transition zone) on gravity and topography should be minimal.

$$v_p = 0.9409 + 2.0947*v_s - 0.8206*v_s^2 + 0.2683*v_s^3 - 0.0251*v_s^4 \quad (12)$$

$$\rho = 1.6612*v_p - 0.4721*v_p^2 + 0.0671*v_p^3 - 0.0043*v_p^4 + 0.000106*v_p^5 \quad (13)$$

The gravity and topography predicted by the initial density model reveal some mismatch with the observations. Figure 3 shows the initial residual gravity up to 80 mGal (Figure 3a), and the initial residual topography, which reaches the value of 0.6 km (Figure 3b). Negative residual gravity indicates that the density constrained by seismic velocity is underestimated, while negative residual topography indicates that the density is mostly overestimated. The primary pattern of the residual gravity and topography is a marked east-west variation. The average residual east of the TGB is not very different from that west of the TGB, so we think the residuals are mostly regional (crustal scale). Refining the density model to reconcile both the residual topography and gravity (within a tolerance margin of 5 mGal and 0.05 km, respectively) can produce a more plausible model of lithospheric density structure.

Figure 4 presents the density distribution at 0–5, 10–15, 20–25, and 30–35 km. At shallow depths (0–5 km), low densities manifest beneath the sedimentary basins, such as the Sichuan basin, Ordos basin, Songliao

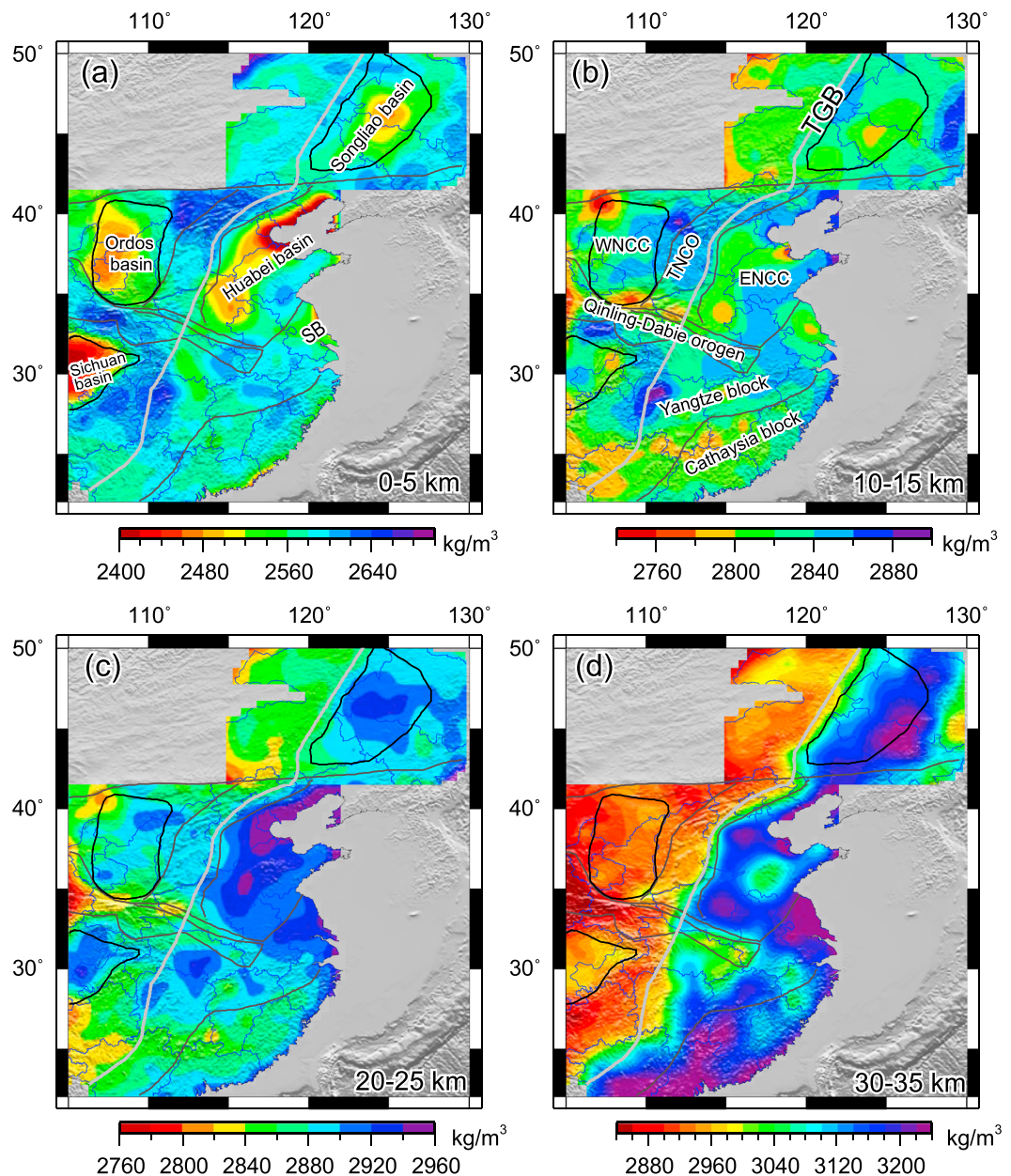


Figure 4. (a) The density of east China at 0–5 km. Prominent basins include JH, Jianghan basin; SB, Subei basin; and EL, Erlian basin. (b–d) Density at 10–15, 20–25, and 30–35 km. Note the bimodal density in Figure 4d, with buoyant material west of the TGB and density lower crust to the east. TGB = topographic gradient belt; ENCC = east north China craton; TNCO = trans-north China orogen; WNCC = west north China craton.

basin, Huabei basin, and Subei basin. By contrast, the TGB coincides with some of the highest density found in eastern China at these depths (Figure 3a).

In the middle and lower crust, more coherent spatial patterns dominate. The Ordos basin, Sichuan basin, Songliao basin, Huabei basin, and Subei basin host the dense material at 20- to 25-km depth. This dichotomy is nearly universal at 30- to 35 km-depth: West of the TGB, densities are mostly lower than $2,960 \text{ kg/m}^3$, compared with the values higher than $3,040 \text{ kg/m}^3$ on the east side.

2.2.2. Crustal Thickness

Our Moho depths are sourced from receiver function estimated in eastern China (Y. Li et al., 2014). Similar to the estimates for crustal densities, crustal thicknesses differ remarkably on the two sides of the TGB

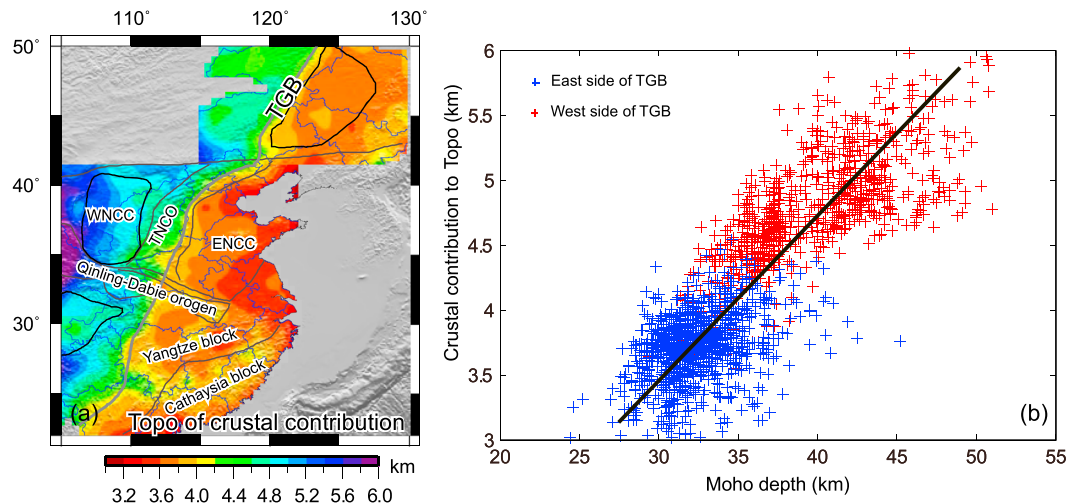


Figure 5. (a) Crustal contribution to topography, H_c . (b) The relationship between Moho depth and crustal topography. The blue and red crosses indicate the values from the east side and west side of TGB, respectively. There is a linear positive relationship between Moho depth and H_c . TGB = topographic gradient belt; ENCC = east north China craton; TNCO = trans-north China orogen; WNCC = west north China craton.

(Figures 2a and 4c). Crustal thickness exceeds 35 km nearly everywhere to the west, and South Qinling has Moho depths of nearly 50 km. By contrast, thicknesses of 30–35 km typify areas to the east of the TGB, and the Songliao basin and the Cathaysia block have Moho depths locally less than 30 km.

2.2.3. Moho Temperature

Sun et al. (2013) estimated the thermal structure of the crust of mainland China by solving the 3-D steady state heat conduction equation using a finite element method in a spherical coordinate system. Additionally, the thermal model was constrained by temperatures inferred from seismic velocities at a depth of 100 km; thermal conductivity and heat production were estimated from P wave velocity, based on empirical formulas. The misfit between the calculated and the observed surface heat flow resulted in an uncertainty of the estimated temperatures of <100 °C (the impacts of which we discuss in section 3.3.2). Moho temperature ranges from 500 °C to 800 °C (Figure 2b). The highest temperatures coincide with volcanoes: the Datong volcano in the NCC, Wudalianchi, and Changbaishan volcano in northeastern China. In addition, the region between the NCC and Tibet also has high temperature, which is consistent with the shear heating due to the continuous Asian-Indian collision (Deng & Tesauro, 2016; Wang et al., 2013).

2.2.4. Elastic Thickness

We derive a 2-D elastic thickness model of the study area (Figure 2c) using the multitaper spectral estimation method of Pérez-Gussinyé et al. (2004). Topography and Bouguer gravity are employed to calculate the coherence with 600 × 600-km window size. The NSGL is generally characterized by low elastic thickness, possibly indicating the inherited weakness proposed by Chen et al. (2013). High elastic thickness is observed in the eastern part of Sichuan Basin, which may indicate the existence of the old cratonic nucleus (Yangtze craton, Chen et al., 2013). The WNCC also appears rigid, which is consistent with the oldest Archean cratons (Kusky et al., 2007). In contrast to these >60-km elastic thicknesses, values of ~15 km characterize the Yangtze and the Cathaysia blocks.

3. Results

3.1. Crustal Contribution to Topography

The density model, especially the crustal component, is refined by our joint inversion of gravity and topography. Figure 5a presents H_c , the crustal contribution to topography. The TGB manifests as a prominent topographic boundary: The region with deep Moho corresponds to high contributions to the topography (Figures 5a and 5b). To the west, H_c generally exceeds 4.2 km and climbs as high as 6.0 km. Yet to the east, values are typically ~3.6 km. East-west transitions of some 1 km over lateral distances of ~200 km are ubiquitous. In most places, the dichotomy in H_c actually overcompensates the difference in surface elevations. That

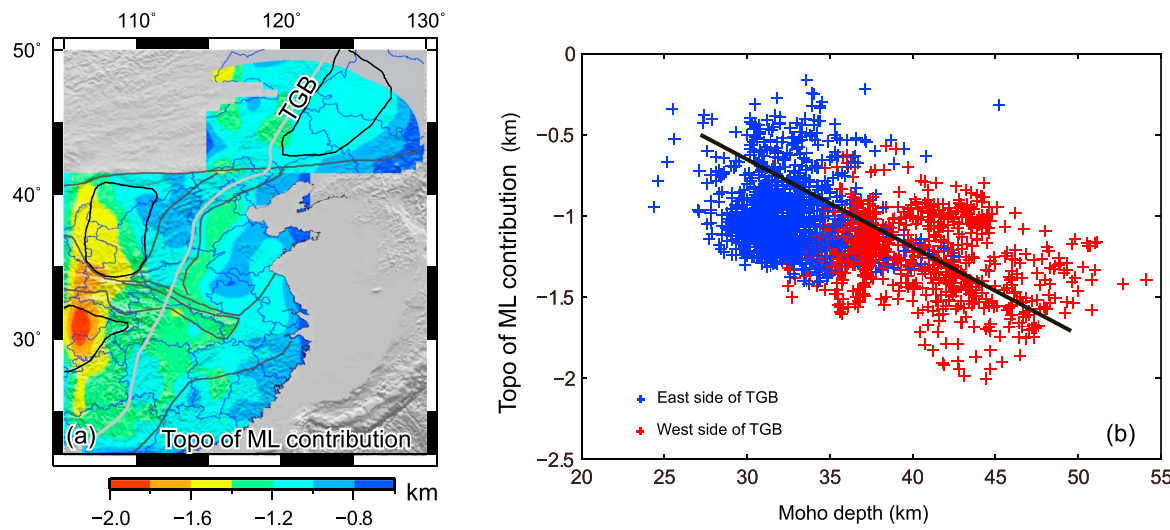


Figure 6. (a) ML contribution to topography, H_{ml} . (b) ML contribution to topography versus Moho depth. The blue and red crosses indicate the values from the east side and west side of TGB, respectively. There is a rough negative relationship between Moho depth and H_{ml} . TGB = topographic gradient belt; ML = mantle lithosphere.

is, the crustal density and Moho depth alone explain the existence of the TGB; we return to this point in section 4.2.

3.2. Mantle Contributions to Topography and Lithospheric Thickness

After accounting for the topographic contribution of the crust, what remains (Figure 6a) is assumed to be due to the ML. West of the TGB, H_{ml} has large-amplitude values (-1.4 km on average). East of the TGB, H_{ml} is less negative (~ -0.8 to -1.2 km), and the Cathaysia block has the minimum mantle contribution ($H_{\text{ml}} \approx -0.6 \text{ km}$). Interestingly, Moho depth has a negative correlation with the topographic contribution (Figure 6b), which confirms the different contributions between the east and the west side of TGB. We will now explore the thickness of ML that would be required if all H_{ml} variations are thermal in origin. Other effects will be discussed in section 4.1.

The average temperature and therefore inferred density of the ML are derived from equations (8) and (11), respectively. As shown in Figure 7, these thermal density estimates occupy a rather narrow range from $3,230$ to $3,250 \text{ kg/m}^3$, with generally—but not uniformly—greater densities east of the TGB. High Moho

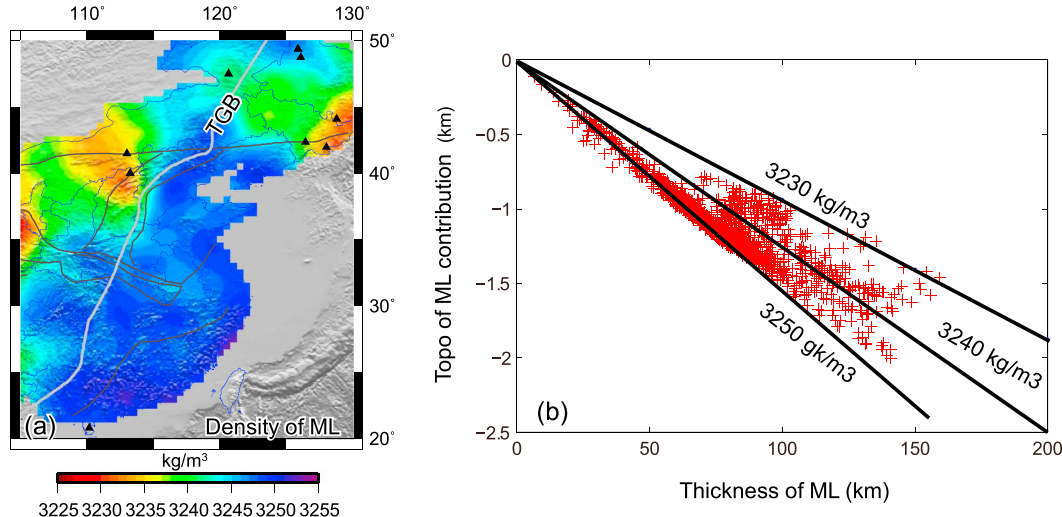


Figure 7. (a) Density of ML. (b) ML contribution to topography versus ML thickness. Three different average ML densities and their contributions to topography are shown in Figure 7b. TGB = topographic gradient belt; ML = mantle lithosphere.

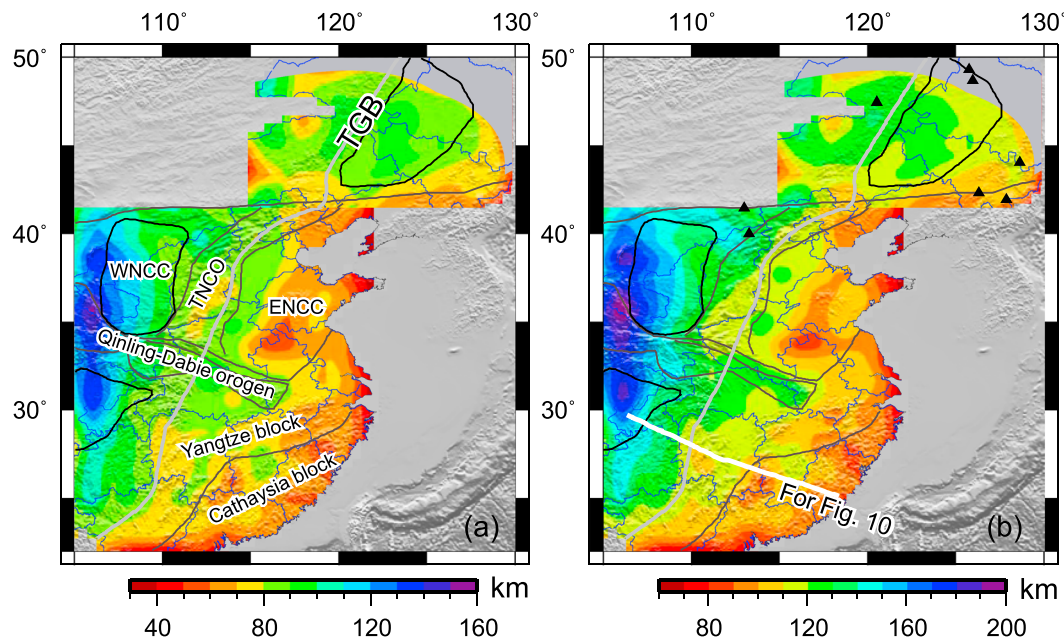


Figure 8. (a) The thickness of ML. (b) Overall lithospheric thickness or the sum of crustal and ML thickness. The black triangle indicates the volcanos. TGB = topographic gradient belt; ENCC = east north China craton; TNCO = trans-north China orogen; WNCC = west north China craton; ML = mantle lithosphere.

temperatures beneath the volcanoes of northern China lead us to estimate high ML temperatures and thus low densities. Other than near volcanic centers, the thicker crust west of the TGB leads to generally higher estimated temperatures at the Moho and therefore higher estimates of ML temperature and estimates of greater ML thickness.

Following this temperature and density estimate, we model a consistent difference across the TGB in ML thickness and especially overall lithospheric thickness (Figure 8). Specifically, the TGB coincides approximately with the contour of 110-km lithospheric thickness, except for the northeastern China and the Qinling-Dabie orogen. The lowest ML and the overall lithospheric thicknesses are found in the southeastern south China and ENCC. The highest thicknesses are present in the Sichuan and Ordos basins, corresponding to the two cratons.

3.3. Uncertainties

3.3.1. Moho Depth

Y. Li et al. (2014) reported that the uncertainty of Moho depth in our study area is typically less than 4 km of the crustal thickness from the RF data. By equation (3), if the density of the lowermost crust is $3,000 \text{ kg/m}^3$ (e.g., Figures 3c and 3d), this 4-km uncertainty produces $\sim 0.13 \text{ km}$ of uncertainty in H_c . By equation (6), this uncertainty could produce 8 km of uncertainty in the final lithospheric thickness. This uncertainty is small compared with the estimated lithospheric thickness. For example, it is $\sim 9\%$ of the lithospheric thickness for the east of the TGB and $<7\%$ of the lithospheric thickness for the west.

3.3.2. Temperature

If only constrained by the measured surface heat flow, the maximum uncertainty of the temperature will reach up to $120\text{--}200^\circ\text{C}$ at a depth of 50 km (Sun et al., 2013). However, Sun et al. estimated the thermal structure by solving the 3-D steady state heat conduction equation and used additional constraints from seismic velocities. Consequently, they claimed that the uncertainty of the estimated Moho temperatures is $<100^\circ\text{C}$, which would change the density of ML by $\pm 6.4 \text{ kg/m}^3$. The corresponding uncertainty of lithospheric thickness resulting from the temperature is shown in Figure 9a. Regions with thick lithosphere have a high uncertainty. For example, the uncertainty on the west side of TGB is $\sim 20 \text{ km}$. On the east side of TGB, the uncertainty is lower than 15 km. Thus, the uncertainty is $\sim 10\%$ of the estimated lithospheric thickness.

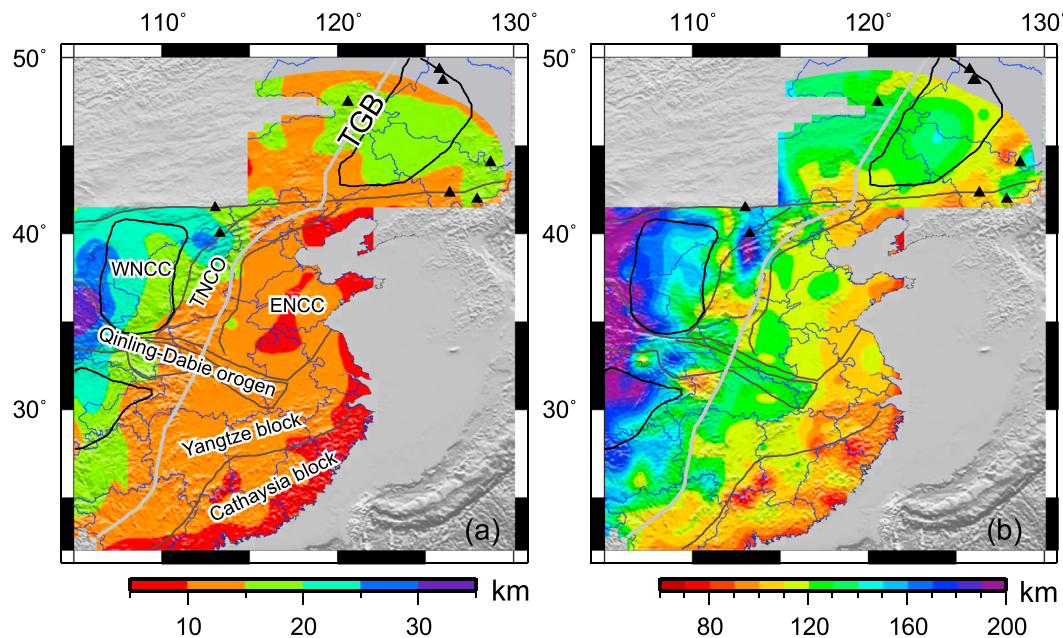


Figure 9. (a) The uncertainty of the crustal contribution on topography according to velocity uncertainties. (b) The lithospheric thickness from local isostasy, which could be an upper bound on thickness from flexure isostasy. The black triangles indicate the volcanoes. TGB = topographic gradient belt; ENCC = east north China craton; TNCO = trans-north China orogen; WNCC = west north China craton.

3.3.3. The Effect of Lithospheric Flexure

It is hard to estimate the uncertainty of elastic thickness (Pérez-Gussinyé et al., 2009), but we attempt to quantify its possible effect by comparing the flexural results with a case of pure local isostasy. The lithospheric thickness from local isostasy (Figure 9b) is similar with the thickness from flexure isostasy. Specifically, ENCC and southeastern south China have thin lithosphere; Orodos and Sichuan basins have thick lithosphere. Nevertheless, ENCC, WNCC, and the Sichuan basin have thinner lithosphere in the case of lithospheric flexure isostasy than local isostasy, due to the high elastic thickness (Figure 2c). We therefore suggest that the thickness from local isostasy is an upper bound on lithospheric thickness in these areas.

4. Discussion

4.1. Other Effects on Topography

Our analysis thus far has been intentionally simplistic. Specifically, we have ignored all aspects of the mantle except for temperature. What we have done, however, has been to uniformly treat the crustal portion of our study area and ascribe the remaining topography to the mantle, be it the temperature or composition/chemistry of the ML or the pattern of flow in the asthenosphere (i.e., dynamic topography). Thus, our estimates of H_{ml} actually represent the sum of the chemical and thermal components of ML buoyancy and any dynamic topography; we have simply quantified what the ML thickness would be if it were isochemical across the region. We now turn our attention to other possible explanations—beyond variations in ML thickness—for the estimated pattern of H_{ml} .

4.1.1. Dynamic Topography

Thus far, our discussion of H_{ml} has assumed that all topography is the result of flexural isostasy. In addition to this component, however, asthenospheric flow may modulate surface elevation of the overriding lithosphere (Flament et al., 2013; Liu, 2015). An asthenospheric upwelling could increase surface elevation, which results in greater lithospheric thickness. On the contrary, an asthenospheric downwelling could result in smaller lithospheric thickness needed to explain topography.

Intraplate volcanism could be the result of upwelling of an anomalously hot mantle plume. In this case, if upwelling affects surface topography, the lithosphere beneath Honggeertu volcano, Dongtong volcano, and Arshan volcano would have to be even thicker than the ~140 km that we model now: rather

counterintuitive for areas of focused intraplate volcanism. Therefore, we suggest that either the upwelling that feeds these volcanoes has a limited impact on surface elevation, or this volcanism is not driven primarily by upwelling.

The region with low lithospheric thickness, mostly located east of the TGB, could be affected by an asthenospheric upwelling, perhaps in the back-arc of the downgoing Pacific plate (Zhao et al., 2011). A large-scale upwelling would require thicker lithosphere in this region, but this would contradict seismological investigations. Chen et al. (2009) and Zheng et al. (2014) have reported low lithospheric thickness (60–70 km) in ENCC, and Q. Li et al. (2013) and Zheng et al. (2014) have observed thin lithosphere in southeastern south China. Therefore, we suggest that the impact of this upwelling on the surface elevation appears to be minor. In summary, we suggest that dynamic topography is limited in east China, consistent with continental and oceanic basin modeling (Wheeler & White, 2002), which jointly analyzed subsidence data from oceanic marginal basins and their fringing continental shelves and suggested subducted slabs have little discernible effect on surface topography across southeast Asia as a whole.

4.1.2. Composition of the ML

Variations in ML composition—especially the degree of melt depletion and associated losses of garnet/spinel and iron—have been proposed to exert an important control on the density (and rheology) of the ML (e.g., Jordan, 1978). As such, one might expect that the NCC may host ML with an element of compositional density or buoyancy. If so, then the ML would have to be thinner or thicker, respectively, in order to produce the estimated total H_{ml} .

To illustrate, melt depletion associated with a 1% increase in Mg# causes a density decrease of $\sim 13 \text{ kg/m}^3$. Thus, if the ML beneath the WNCC (thermal density $\sim 3,240 \text{ kg/m}^3$) is 1% Mg enriched, then its density would be $3,227 \text{ kg/m}^3$. Instead of $\sim 110 \text{ km}$, the ML would have to be $\sim 160 \text{ km}$ thick to have the same $-1.4 \text{ km } H_{ml}$.

Nevertheless, the alteration documented in the ENCC includes large-scale refertilization (e.g., Deng et al., 2013; Zheng et al., 2007). Modeling of olivine-Mg# in peridotites also proposes fertile mantle in the ENCC (Guo et al., 2016). If so, the density of ML in the ENCC is greater than our purely thermal estimate, and the lithosphere could be thinner than that estimated from equation (1)–(13) and shown in Figure 8. Furthermore, because there are many similarities (e.g., elevation, crustal thickness, lithospheric thickness, and heat flow) between the ENCC and other areas east of the TGB, one may speculate that similar processes affected this entire region. In this case, the systematic drop in ML thickness across the TGB may be even more pronounced than estimated above. Following similar logic as in the previous paragraph, a 2% decrease in Mg# (Zheng et al., 2007) would decrease the thickness of typical lithospheric thickness from ~ 90 to $\sim 70 \text{ km}$ (calculated for ML $3,250 \text{ kg/m}^3$ and $H_{ml} = 1 \text{ km}$), which in turn seems to support the estimation of #Mg (Guo et al., 2016).

4.1.3. Hydration of the ML

Seismic tomography shows a distinct low-velocity mantle wedge in east China (Huang & Zhao, 2006; Zhao et al., 2011). This anomaly was first proposed to be the result of the dehydration of the subducted Pacific slab and ensuing hydration of overlying mantle. Such hydration may have induced intracontinental basaltic magmatism in east China (e.g., Kuritani et al., 2011; Kusky et al., 2014; Wang et al., 2015; Zhao et al., 2009).

As with melt-depletion, hydration-induced retrogression of the ML reduces density. According to our calculations, we find a thinner lithosphere to the east of TGB. To illustrate the possible effect of hydration-induced retrogression, we take -1 km as a representative average H_{ml} in the areas east of the TGB. Here we estimated an ML density and thickness of $3,250 \text{ kg/m}^3$ and $\sim 60 \text{ km}$. A crude estimate—for illustrative purposes only—of the effect of hydration on density is derived from Christensen (2004, Figure 1 therein): 1% serpentinization of peridotite causes an 8 kg/m^3 decrease in density. Similar values can be obtained for addition of hydrous products to normally anhydrous ML lithologies using the database of Hacker and Abers (2004). Thus, if the ML easternmost of the TGB contains 1% serpentinite, the $+50 \text{ kg/m}^3$ density contrast with asthenosphere would decrease to $+42 \text{ kg/m}^3$, and the necessary thickness of lithosphere would increase from 90 to $\sim 100 \text{ km}$. We conclude that hydration-induced density loss east of the TGB could diminish the discrepancy in ML thickness.

In addition to systematic biases introduced by dynamic topography, composition, and hydration, we note that we use Moho temperatures constrained by heat flow and seismic velocity, but these temperatures are derived from the steady state equation. Thermal structure in tectonically active regions could possibly be

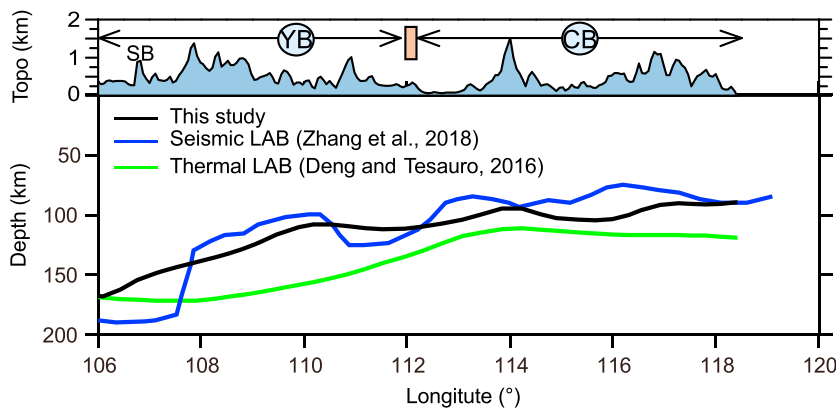


Figure 10. The comparison of the lithosphere-asthenosphere boundary (LAB) depths along a profile in south China. YB = Yangtze block; CB = Cathaysia block; SB = Sichuan basin. The location of the profile is outlined in Figure 8b.

far from steady state, which may bias the final estimates. However, Sun et al. (2013) state that their model is applicable in mainland China. Notably, even in Tibet and Baikal Rift Zone, their model is comparable with that from petrologic and non–steady state geothermal constraints (Sun et al., 2013).

4.2. Geodynamic Implications of Lithospheric Thickness Patterns

Broadly, the ML and lithosphere are thicker to the west of the TGB than to the east (Figure 8). Lithospheric extension and thinning has been previously documented in the ENCC, and the westward subducted Pacific plate has been implicated in this process (Chen et al., 2008; Ren et al., 2002; Sun et al., 2007; Zhu et al., 2012). Other seismic data provide evidence of lithospheric modification beneath much of eastern China (H. Li et al., 2018; X. Li et al., 2015; Wang et al., 2017; Zhang et al., 2014; Zheng et al., 2014). Our results provide a broad view of lithospheric thickness and support the proposed lithospheric dismemberment in east China.

Our isostatic lithosphere is not everywhere the same of seismic estimates, but spatial trends are similar. For example, in the NCC we estimate ~90 km, which is greater than the 60–70 km modeled by Chen (2010) and Zheng et al. (2014). Both models, however, show thin lithosphere in the ENCC but high values in the north part of the TNCO and in the WNCC. South of TNCO, the lithosphere is thinner (110–120 km) than to the north (>120 km). Additionally, the thickness in the southern TNCO is consistent with that estimated from active-source seismic work (S. Li et al., 2011) and the depth of a midlithospheric discontinuity (Chen et al., 2014). In south China, even though the isostatic lithospheric thickness is less than the thermal lithosphere, our lithospheric thickness is comparable to seismic results (Zhang et al., 2018), and both feature increasing depth from the coast to the interior mainland (Figure 10), although our results are smoother than those of Zhang et al. (2018).

Nevertheless, it is curious that the isostatic lithospheric thickness is not exactly the same as the seismic lithosphere. Composition and fluid could affect the density estimation and therefore the isostatic lithospheric thickness (section 4.2). For example, as proposed by Hu et al. (2018), the ML could be compositional denser than a pure thermal lithosphere. In that case, the isostatic lithosphere could be better match to that from seismic data. However, as noted by previous studies (e.g., Globig et al., 2016; Gvirtzman et al., 2016; Robert et al., 2015), the isostatic lithosphere needs not be the same as the thermal lithosphere (i.e., the depth range over which conductive heat transfer dominates) or seismic lithosphere (above the low-velocity zone). Future and ongoing multidisciplinary studies offer a promising way to probe the physical and chemical properties of in situ upper mantle.

Zhang et al. (2014) analyzed S-receiver functions from across northeastern China and found thinner lithosphere inside the Songliao basin (as shallow as ~100 km, with an average ML thickness of ~85 km) relative to nearby regions, which is opposite our lithospheric thickness map (Figures 8b). In addition to this seismic estimate, magnetotelluric tomography suggests a high-conductivity layer as shallow as 60 km beneath the Songliao basin (Liu et al., 2006). There are two explanations for the disagreement between our estimate and these others. In our analysis, a high modeled Moho temperature in the Songliao basin leads us to

estimate a low ML density and therefore requires a thick isostatic lithosphere; a lower Moho temperature would bring our results closer to others. Alternatively, the ML could indeed be thinner if it is more fertile and thus compositionally dense (but still warm).

4.3. The Origin of Topographic Support for the TGB

As discussed above, the jump in elevation across the TGB is due to crustal buoyancy. In fact, H_c increases even more dramatically to the west than does surface elevation: We find that the ML actually counters the crustal contribution to topography. If the lithosphere were the same thickness and density east of the TGB, the elevation contrast would be even greater.

By accounting for H_c and using existing estimates of Moho temperature, we quantify the variations in ML thickness that would be necessary if the only contribution to H_{ml} is from the temperature of the ML relative to the asthenosphere. To a large extent, the variations in this approximation are reasonable and mirror (albeit imperfectly) thickness variations obtained using other proxies.

Specific to the TGB, any (upward) dynamic topography or compositional buoyancy west of the belt would require even thicker ML, beyond the limits that are normally estimated even for Archean cratons. Therefore, we posit that the thick root that we image is thermal in origin. By contrast, if the low-elevation areas east of the TGB are subject to downward pull or refertilization, the ML would be even thinner.

5. Conclusions

We aim to understand the tectonic evolution and current topography of eastern China, the site of both globally important tectonic processes such as craton destruction and widespread intracontinental magmatism. To do so, we use surface topography as geophysical data and first strip away the crustal contribution to elevation, leaving behind the combined effects of mantle temperature, composition, and asthenospheric flow. A sharp divide exists between thick, dry lithosphere (>120 km) beneath central China and thin lithosphere (~90 km) beneath easternmost China. The consistency of this dichotomy from north to south suggests that not only previously cratonic terranes but also easternmost China as a whole has undergone lithospheric dismemberment. Mantle refertilization in easternmost China would accentuate the dichotomy in lithospheric thickness, whereas hydration-induced density loss above the subducting Pacific plate may reduce it. Widespread dynamic topography seems unlikely in the study area. Upward flow beneath the easternmost China would magnify the difference with seismic results in lithospheric thickness. Similarly, the intraplate volcanism may be fed by asthenospheric upwelling, but if there is any topographic contribution from this upwelling, the ML in these areas of focused magmatism would have to be—quite puzzlingly—anomalously thick.

Acknowledgments

We are very grateful to Weisen Shen for providing us his seismic velocity model. We thank Yigang Xu and Yun Chen for valuable discussions. Constructive comments from Editor Nathan A. Niemi, the Associate Editor, and two anonymous reviewers have greatly improved the manuscript. The data used in this paper are available from <https://github.com/sissiautumn/Deng>. This research was funded by the National Key R&D Program of China (grant 2016YFC0600402), the Strategic Priority Research Program (B) of the Chinese Academy of Sciences (grant XDB18000000), Youth Innovation Promotion Association CAS (YIPA), and Tuguangchi Award for Excellent Young Scholar (TGC201702).

References

- Amante, C., & Eakins, B. W. (2009). ETOPO1 1 arc-minute global relief model: Procedures, data sources and analysis. NOAA Technical Memorandum NESDIS NGDC-24. National Geophysical Data Center, NOAA. <https://doi.org/10.7289/V5C8276M>
- Brocher, T. M. (2005). Empirical relations between elastic wavespeeds and density in the Earth's crust. *Bulletin of the Seismological Society of America*, 95(6), 2081–2092. <https://doi.org/10.1785/0120050077>
- Chen, B., Chen, C., Kaban, M. K., Du, J., Liang, Q., & Thomas, M. (2013). Variations of the effective elastic thickness over China and surroundings and their relation to the lithosphere dynamics. *Earth and Planetary Science Letters*, 363, 61–72. <https://doi.org/10.1016/j.epsl.2012.12.022>
- Chen, L. (2010). Concordant structural variations from the surface to the base of the upper mantle in the north China craton and its tectonic implications. *Lithos*, 120(1–2), 96–115. <https://doi.org/10.1016/j.lithos.2009.12.007>
- Chen, L., Cheng, C., & Wei, Z. G. (2009). Seismic evidence for significant lateral variations in lithospheric thickness beneath the central and western north China craton. *Earth and Planetary Science Letters*, 286(1–2), 171–183. <https://doi.org/10.1016/j.epsl.2009.06.022>
- Chen, L., Jiang, M., Yang, J., Wei, Z., Liu, C., & Ling, Y. (2014). Presence of an intralithospheric discontinuity in the central and western north China craton: Implications for destruction of the craton. *Geology*, 42(3), 223–226. <https://doi.org/10.1130/G35010.1>
- Chen, L., Tao, W., Zhao, L., & Zheng, T. (2008). Distinct lateral variation of lithospheric thickness in the northeastern north China craton. *Earth and Planetary Science Letters*, 267(1–2), 56–68. <https://doi.org/10.1016/j.epsl.2007.11.024>
- Christensen, N. I. (2004). Serpentinites, peridotites, and seismology. *International Geology Review*, 46(9), 795–816. <https://doi.org/10.2747/0020-6814.46.9.795>
- Deng, Y., Fan, W., Zhang, Z., & Badal, J. (2013). Geophysical evidence on segmentation of the Tancheng-Lujiang fault and its implications on the lithosphere evolution in East China. *Journal of Asian Earth Sciences*, 78, 263–276. <https://doi.org/10.1016/j.jseaes.2012.11.006>
- Deng, Y., Levandowski, W., & Kusky, T. (2017). Lithospheric density structure beneath the Tarim basin and surroundings, northwestern China, from the joint inversion of gravity and topography. *Earth and Planetary Science Letters*, 460, 244–254. <https://doi.org/10.1016/j.epsl.2016.10.051>
- Deng, Y., & Tesauro, M. (2016). Lithospheric strength variations in mainland China: Tectonic implications. *Tectonics*, 35, 2313–2333. <https://doi.org/10.1002/2016TC004272>
- Flament, N., Gurnis, M., & Müller, R. D. (2013). A review of observations and models of dynamic topography. *Lithosphere*, 5(2), 189–210. <https://doi.org/10.1130/L245.1>

- Foley, S. F. (2008). Rejuvenation and erosion of the cratonic lithosphere. *Nature Geoscience*, 1(8), 503–510. <https://doi.org/10.1038/ngeo261>
- Gao, S., Zhang, J., Xu, W., & Liu, Y. (2009). Delamination and destruction of the north China craton. *Chinese Science Bulletin*, 54(19), 3367–3378. <https://doi.org/10.1007/s11434-009-0395-9>
- Globig, J., Fernández, M., Torne, M., Vergés, J., Robert, A., & Faccenna, C. (2016). New insights into the crust and lithospheric mantle structure of Africa from elevation, geoid, and thermal analysis. *Journal of Geophysical Research: Solid Earth*, 121, 5389–5424. <https://doi.org/10.1002/2016JB012972>
- Guo, Z., Afonso, J. C., Qashqai, M. T., Yang, Y., & Chen, Y. J. (2016). Thermochemical structure of the north China craton from multi-observable probabilistic inversion: Extent and causes of cratonic lithosphere modification. *Gondwana Research*, 37, 252–265. <https://doi.org/10.1016/j.gr.2016.07.002>
- Gvirtzman, Z., Faccenna, C., & Becker, T. W. (2016). Isostasy, flexure, and dynamic topography. *Tectonophysics*, 683, 255–271. <https://doi.org/10.1016/j.tecto.2016.05.041>
- Hacker, B. R., & Abers, G. A. (2004). Subduction factory 3: An excel worksheet and macro for calculating the densities, seismic wave speeds, and H₂O contents of minerals and rocks at pressure and temperature. *Geochemistry, Geophysics, Geosystems*, 5, Q01005. <https://doi.org/10.1029/2003GC000614>
- Hu, J., Liu, L., Faccenda, M., Zhou, Q., Fischer, K. M., Marshak, S., et al. (2018). Modification of the western Gondwana craton by plume–lithosphere interaction. *Nature Geoscience*, 11(3), 203–210. <https://doi.org/10.1038/s41561-018-0064-1>
- Huang, J., & Zhao, D. (2006). High-resolution mantle tomography of China and surrounding regions. *Journal of Geophysical Research*, 111, B09305. <https://doi.org/10.1029/2005JB004066>
- Jiang, G., Guo, P., Rao, S., Zhang, L., Tang, X., Huang, F., et al. (2016). Compilation of heat flow data in the continental area of China (4th edition). *Chinese Journal of Geophysics*, 59(8), 2892–2910. <https://doi.org/10.6038/cjg20160815>
- Jordan, T. H. (1978). Composition and development of the continental tectosphere. *Nature*, 274(5671), 544–548. <https://doi.org/10.1038/274544a0>
- Katsura, T., Shatskiy, A., Manthilake, M. G. M., Zhai, S., Fukui, H., Yamazaki, D., et al. (2009). Thermal expansion of forsterite at high pressures determined by in situ X-ray diffraction: The adiabatic geotherm in the upper mantle. *Physics of the Earth and Planetary Interiors*, 174(1–4), 86–92. <https://doi.org/10.1016/j.pepi.2008.08.002>
- King, S. D., Frost, D. J., & Rubie, D. C. (2015). Why cold slabs stagnate in the transition zone. *Geology*, 43(3), 231–234. <https://doi.org/10.1130/G36320.1>
- Kuritani, T., Ohtani, E., & Kimura, J.-I. (2011). Intensive hydration of the mantle transition zone beneath China caused by ancient slab stagnation. *Nature Geoscience*, 4(10), 713–716. <https://doi.org/10.1038/ngeo1250>
- Kusky, T., Windley, B., & Zhai, M.-G. (2007). Lithospheric thinning in eastern Asia: constraints, evolution, and tests of models. *Geological Society, London, Special Publications*, 280(1), 331–343. <https://doi.org/10.1144/SP280.18>
- Kusky, T. M., Windley, B. F., Wang, L., Wang, Z., Li, X., & Zhu, P. (2014). Flat slab subduction, trench suction, and craton destruction: Comparison of the north China, Wyoming, and Brazilian cratons. *Tectonophysics*, 630, 208–221. <https://doi.org/10.1016/j.tecto.2014.05.028>
- Lachenbruch, A. H., & Morgan, P. (1990). Continental extension, magmatism and elevation: formal relations and rules of thumb. *Tectonophysics*, 174(1), 39–62. [https://doi.org/10.1016/0040-1951\(90\)90383-J](https://doi.org/10.1016/0040-1951(90)90383-J)
- Levandowski, W., Boyd, O. S., Briggs, R. W., & Gold, R. D. (2015). A random-walk algorithm for modeling lithospheric density and the role of body forces in the evolution of the midcontinent rift. *Geochemistry, Geophysics, Geosystems*, 16, 4084–4107. <https://doi.org/10.1002/2015GC005961>
- Li, Q., Gao, R., Wu, F. T., Guan, Y., Ye, Z., Liu, Q., et al. (2013). Seismic structure in the southeastern China using teleseismic receiver functions. *Tectonophysics*, 606, 24–35. <https://doi.org/10.1016/j.tecto.2013.06.033>
- Li, H., Song, X., Lü, Q., Yang, X., Deng, Y., Ouyang, L., et al. (2018). Seismic imaging of lithosphere structure and upper mantle deformation beneath east-central China and their tectonic implications. *Journal of Geophysical Research: Solid Earth*, 123, 2856–2870. <https://doi.org/10.1002/2017JB014992>
- Li, S., Lai, X., Liu, B., Wang, Z., He, J., & Sun, Y. (2011). Differences in lithospheric structures between two sides of Taihang Mountain obtained from the Zhucheng-Yichuan deep seismic sounding profile. *Science China Earth Sciences*, 54(6), 871–880. <https://doi.org/10.1007/s11430-011-4191-4>
- Li, X., Zhu, P., Kusky, T. M., Gu, Y., Peng, S., Yuan, Y., et al. (2015). Has the Yangtze craton lost its root? A comparison between the north China and Yangtze cratons. *Tectonophysics*, 655, 1–14. <https://doi.org/10.1016/j.tecto.2015.04.008>
- Li, Y., Gao, M., & Wu, Q. (2014). Crustal thickness map of the Chinese mainland from teleseismic receiver functions. *Tectonophysics*, 611, 51–60. <https://doi.org/10.1016/j.tecto.2013.11.019>
- Liu, G. X., Zhang, Z. H., Han, J. T., & Tang, J. H. (2006). Features of the electric structure of the lithosphere beneath the Hinggan–Inner Mongolia and Jilin–Heilongjiang regions. *Geology in China*, 33(4), 824–831. (in Chinese with English abstract)
- Liu, L. (2015). The ups and downs of North America: Evaluating the role of mantle dynamic topography since the Mesozoic. *Reviews of Geophysics*, 53, 1022–1049. <https://doi.org/10.1002/2015RG000489>
- Menzies, M. A., & Xu, Y. (1998). Geodynamics of the north China craton. *Geodynamics Series*, 27, 155–165. <https://doi.org/10.1029/GD027p0155>
- Parsons, B., & Sclater, J. G. (1977). An analysis of the variation of ocean floor bathymetry and heat flow with age. *Journal of Geophysical Research*, 82(5), 803–827. <https://doi.org/10.1029/JB082i005p00803>
- Pavlis, N. K., Holmes, S. A., Kenyon, S. C., & Factor, J. K. (2012). The development and evaluation of the Earth Gravitational Model 2008 (EGM2008). *Journal of Geophysical Research*, 117, B04406. <https://doi.org/10.1029/2011JB008916>
- Pérez-Gussinyé, M., Lowry, A. R., Watts, A. B., & Velicogna, I. (2004). On the recovery of effective elastic thickness using spectral methods: Examples from synthetic data and from the Fennoscandian Shield. *Journal of Geophysical Research*, 109, B10409. <https://doi.org/10.1029/2003JB002788>
- Pérez-Gussinyé, M., Swain, C., Kirby, J., & Lowry, A. (2009). Spatial variations of the effective elastic thickness, Te, using multitaper spectral estimation and wavelet methods: Examples from synthetic data and application to South America. *Geochemistry, Geophysics, Geosystems*, 8, Q05009. <https://doi.org/10.1029/2006GC001511>
- Ren, J., Tamaki, K., Li, S., & Junxia, Z. (2002). Late Mesozoic and Cenozoic rifting and its dynamic setting in eastern China and adjacent areas. *Tectonophysics*, 344(3–4), 175–205. [https://doi.org/10.1016/S0040-1951\(01\)00271-2](https://doi.org/10.1016/S0040-1951(01)00271-2)
- Robert, A., Fernández, M., Jiménez-Munt, I., & Vergés, J. (2015). Lithospheric structures in central Eurasia derived from elevation, geoid anomaly and a thermal analysis. *Geological Society - Special Publications*, 427(1), 271–293. <https://doi.org/10.1144/SP427.10>
- Shen, W., Ritzwoller, M. H., Kang, D., Kim, Y., Lin, F.-C., Ning, J., et al. (2016). A seismic reference model for the crust and uppermost mantle beneath China from surface wave dispersion. *Geophysical Journal International*, 206(2), 954–979. <https://doi.org/10.1093/gji/ggw175>

- Sun, W., Ding, X., Hu, Y.-H., & Li, X.-H. (2007). The golden transformation of the Cretaceous plate subduction in the west Pacific. *Earth and Planetary Science Letters*, 262(3–4), 533–542. <https://doi.org/10.1016/j.epsl.2007.08.021>
- Sun, Y., Dong, S., Zhang, H., Li, H., & Shi, Y. (2013). 3D thermal structure of the continental lithosphere beneath China and adjacent regions. *Journal of Asian Earth Sciences*, 62, 697–704. <https://doi.org/10.1016/j.jseaes.2012.11.020>
- Wang, C.-Y., Chen, W.-P., & Wang, L.-P. (2013). Temperature beneath Tibet. *Earth and Planetary Science Letters*, 375, 326–337. <https://doi.org/10.1016/j.epsl.2013.05.052>
- Wang, Q., Song, X., & Ren, J. (2017). Ambient noise surface wave tomography of marginal seas in East Asia. *Earth and Planetary Physics*, 1(1), 13–25. <https://doi.org/10.26464/epp2017003>
- Wang, X.-C., Wilde, S. A., Li, Q.-L., & Yang, Y.-N. (2015). Continental flood basalts derived from the hydrous mantle transition zone. *Nature Communications*, 6(1), 7700. <https://doi.org/10.1038/ncomms8700>
- Watts, A. B. (2001). *Isostasy and flexure of the lithosphere*. Cambridge: Cambridge University Press.
- Wheeler, P., & White, N. (2002). Measuring dynamic topography: An analysis of Southeast Asia. *Tectonics*, 21(5), 1040. <https://doi.org/10.1029/2001TC900023>
- Xu, Y. G. (2007). Diachronous lithospheric thinning of the north China craton and formation of the Daxin'anling-Taihangshan gravity lineament. *Lithos*, 96(1–2), 281–298. <https://doi.org/10.1016/j.lithos.2006.09.013>
- Zhang, H.-F. (2005). Transformation of lithospheric mantle through peridotite-melt reaction: A case of Sino-Korean craton. *Earth and Planetary Science Letters*, 237(3–4), 768–780. <https://doi.org/10.1016/j.epsl.2005.06.041>
- Zhang, R., Wu, Q., Sun, L., He, J., & Gao, Z. (2014). Crustal and lithospheric structure of northeast China from S-wave receiver functions. *Earth and Planetary Science Letters*, 401, 196–205. <https://doi.org/10.1016/j.epsl.2014.06.017>
- Zhang, Y. Y., Chen, L., Ai, Y. S., Jiang, M. M., Xu, W. W., & Shen, Z. Y. (2018). Lithospheric structure of the south China block from S-receiver function. *Chinese Journal of Geophysics*, 61(1), 138–149. <https://doi.org/10.6038/cjg2018L0226>
- Zhao, D., Tian, Y., Lei, J., Liu, L., & Zheng, S. (2009). Seismic image and origin of the Changbai intraplate volcano in East Asia: Role of big mantle wedge above the stagnant Pacific slab. *Physics of the Earth and Planetary Interiors*, 173(3–4), 197–206. <https://doi.org/10.1016/j.pepi.2008.11.009>
- Zhao, D., Yu, S., & Ohtani, E. (2011). East Asia: Seismotectonics, magmatism and mantle dynamics. *Journal of Asian Earth Sciences*, 40(3), 689–709. <https://doi.org/10.1016/j.jseaes.2010.11.013>
- Zheng, J., Griffin, W., O'Reilly, S. Y., Yu, C., Zhang, H., Pearson, N., et al. (2007). Mechanism and timing of lithospheric modification and replacement beneath the eastern north China craton: Peridotitic xenoliths from the 100 Ma Fuxin basalts and a regional synthesis. *Geochimica et Cosmochimica Acta*, 71(21), 5203–5225. <https://doi.org/10.1016/j.gca.2007.07.028>
- Zheng, T.-Y., Zhao, L., He, Y.-M., & Zhu, R.-X. (2014). Seismic imaging of crustal reworking and lithospheric modification in eastern China. *Geophysical Journal International*, 196(2), 656–670. <https://doi.org/10.1093/gji/gjt420>
- Zhu, R., Xu, Y., Zhu, G., Zhang, H., Xia, Q., & Zheng, T. (2012). Destruction of the north China craton. *Science China Earth Sciences*, 55(10), 1565–1587. <https://doi.org/10.1007/s11430-012-4516-y>